Prediction of Damage Evolution in Composites Using Abaqus

W. Wilson

Fokker Landing Gear B.V., The Netherlands

Abstract: Fokker Landing Gear has a history in development of composite technology for landing gear applications. In order to successfully design and qualify composite landing gear parts it is essential to be able to reliable predict the mechanical and failure behavior of the material.
With traditional composite material models the mechanical behavior and failure moment of thin and undisturbed composite sections can be predicted relatively well. However, for thick composites and around stress concentration (e.g. open holes, pin loaded holes) these models substantially underpredict measured failure loads.
In recent years Fokker Landing Gear has developed a proprietary material model to more accurately model composites. In this material model the fibers and resin are included as separate materials with their own specific material and failure behavior, both with a limited number of material parameters and with clear physical meaning. The interaction between the fibers and resin is accounted for using a new analytical approach. Because the inclusion of fibers is done using a vector based approach the model is valid for any fiber structure.
In the current study this material model has been extended to also include non-local damage mechanics (including damage evolution), and more realistic (physics based) damage laws for fiber damage. Also a new damage initiation criterion for the onset of damage in cohesive surfaces (delaminations) based on both transverse shear stresses and out-of-plane stresses has been added. The implementation of this material model and cohesive damage laws is done in Abaqus/Standard. The extended material model can now also accurately predict the moment of failure and failure mode around stress concentrations.

Keywords: Composites, Constitutive Model, Damage, Delamination, Fabrics, Failure, Landing Gear, User-Defined Material,

1. Introduction

Fokker Landing Gear has a history in the development of composite technology development for landing gear applications (Figure 1). To be able to design and qualify composite landing gear parts it is essential to be able to reliable predict the mechanical and failure behavior of the material.
Traditional models are in most cases linear elastic and use failure criteria (in most cases only valid for uni-directional materials) to predict the moment of failure. Hence, they do not take into account the nonlinear behavior of the resin and the actual damage initiation and damage evolution. With these traditional models the mechanical behavior and failure moment of thin undisturbed composite sections can be predicted relatively well. However, for thick composites and especially around stress concentration (e.g. open holes, pin loaded holes) the traditional models under predict the failure loads by a large margin (e.g. Chang et al., 1984; Whitworth et al., 2003).

Figure 1. Examples of composite landing gear parts developed by Fokker Landing Gear. Left) Composite drag brace for a large commercial aircraft. Right) Composite trailing arm for the NH90 Helicopter.

In recent years Fokker Landing Gear has developed their own material model for modeling composites (Wilson, 2011). In this material model fibers and resin are included as separate materials with their own specific material and failure behavior, both with a limited number of required material parameters. The interaction between the fibers and resin is accounted for using a new analytical approach. Because the inclusion of fibers is done using a vector based approach the model is valid for any fiber structure. We have previously shown that composites consisting of 2x2 twill fabrics layers and composites consisting of braid layers (with varying angles) can be described with the same set of material data (Wilson, 2011).

The goal of the current study is to extend this model such that is can also accurately predict the failure of composites around stress concentrations. For this purpose we have extended the material model to include non-local damage mechanics (including damage evolution), and more realistic (physics based) damage laws for (compressive) fiber damage. A new damage initiation criterion for the onset of damage in cohesive surfaces (delaminations), based on both transverse shear stresses and out-of-plane stresses has been added. The new material model and cohesive damage laws have been implemented in Abaqus/Standard using the Abaqus user-subroutines UMAT, URDFLD UVARM, URDFIL and UFIELD.

In the current study the model predictions of the new version of this model were compared to the mechanical and failure behavior of in-plane shear and interlaminar shear coupon tests, and bearing and open-hole compression elements tests.

2. Method

2.1 Material model

2.1.1 Total stress

The total stress in the material is given by

$$\boldsymbol{\sigma}_{tot} = \left(1 - \sum_{i=1}^{totf} \rho_f^i\right)\boldsymbol{\sigma}_r + \sum_{i=1}^{totf} \rho_f^i \boldsymbol{\sigma}_f^i \text{ ,} \quad \text{Equation 1}$$

where $\boldsymbol{\sigma}_r$ and $\boldsymbol{\sigma}_f$ are the total resin and fiber stress tensors, respectively, and ρ_f^i and σ_f^i are the volume fraction and fiber stress in the *i*-th direction $\vec{e}_f^{\,i}$, respectively. When the strains in a composite are relatively low, it can be assumed that the relative volume fractions of the resin and fiber stay constant during deformation. Hence, ρ_f^i is taken as a constant. Before occurring of damage in the material both the resin and fiber are assumed to behave linear elastic.

2.1.2 Microstructure model

A fiber-reinforced composite consists of fibers embedded in a resin. When loaded all loads are distributed between the fibers and resin. This means that the total amount of stress in the composite is equal to the sum of all stresses in the resin and fibers. The same hold for strains.

The distribution of the total strain over the fibers and resin depends on the stiffness of the two components, their relative volume fractions and the microstructure of the composite. If we for instance look at a composite of which the resin stiffness is much lower than the fiber stiffness, the resin strain in the direction perpendicular to the fiber-direction will be much larger than the fiber strain.

In the material model this distribution of stresses and strains between the resin and fibers is included using an analytical representation of the microstructure. This done by writing the fiber stress tensor $\boldsymbol{\sigma}_f$ as a function of the resin stress tensor $\boldsymbol{\sigma}_r$. The equations to couple the fiber and resin stress tensor are proprietary to Fokker Landing Gear.

2.1.3 Fiber directions and properties

Fiber directions are included as vectors $\vec{e}_f^{\,i}$. The current fiber direction can be written as a function of the deformation gradient tensor (**F**) and the initial fiber direction ($\vec{e}_{f,0}^{\,i}$) as

$$\vec{e}_f^{\,i} = \frac{\mathbf{F} \cdot \vec{e}_{f,0}^{\,i}}{\left\| \mathbf{F} \cdot \vec{e}_{f,0}^{\,i} \right\|} \text{.} \quad \text{Equation 2}$$

The logarithmic fiber strains in fiber direction can be computed as

$$\varepsilon_f^i = \vec{e}_f^{\,i} \cdot \boldsymbol{\varepsilon}_{\mathrm{tot}} \cdot \vec{e}_f^{\,i}, \text{ Equation 3}$$

where $\boldsymbol{\varepsilon}_{\mathrm{tot}}$ is the strain tensor of the composite.

As mentioned above, the fibers are assumed to behave linear elastic. However, the fibers are assumed to have a different stiffness in compression and tension, as

$$\begin{aligned} E_f &= E_{ft} \quad \text{for} \quad \varepsilon_f \geq 0 \\ E_f &= E_{fc} \quad \text{for} \quad \varepsilon_f < 0 \end{aligned}. \text{ Equation 4}$$

2.1.4 Failure behavior

Fiber damage is assumed to be a brittle fracture. Although it is assumed that a fiber fails immediately once damaged, the total damage in a fiber bundle is assumed to evolve more gradually, this mainly due to the differences in fiber orientations and resin distribution around the fibers (which influences the local fiber stresses). The following function for the evolution of the damage parameter D_f is used

$$D_f = \left(\frac{\kappa_{c,f}}{\kappa_f}\right)\left(\frac{\kappa_f - \kappa_{i,f}}{\kappa_{c,f} - \kappa_{i,f}}\right). \text{ Equation 5}$$

$\kappa_{i,f}$ and $\kappa_{c,f}$ are the values of history parameter κ_f at which damage initiation starts and at which the fibers have completely failed. For tensile failure the history parameter κ_f is set equal to the maximum fiber strain over time. The function for κ used for compressive failure is proprietary to Fokker Landing gear, but is based on the assumption that fiber buckling is dependent on the compressive fiber strain, resin stiffness and resin damage (the resin supports the fibers) and the out-of-plane stress (compressive out-of-plane stresses are assumed to inhibit micro-buckling and tensile out-of-plane stresses are assumed to promote micro-buckling).

It is assumed that resin damage will in most cases start around fibers at locations where there are high strain concentrations. As these local strains concentrations can be much larger than the average resin strain, initial damage can start at relatively low average resin strains. As this initial damage is very local it is assumed to hardly affect the overall stiffness. Due to this the damage evolution speeds will be very low just after damage initiation. Only when the amount of damage becomes significant the speed of damage evolution will increase rapidly. This means that the process of damage progression takes place relatively slow, and that there is a large difference between the composite strain at which resin damage is initiated and the strain at which it completely fails. The equation to model damage progression is proprietary to Fokker Landing Gear and is therefore not given here.

When the resin is damaged it is assumed to slowly crumble. This means that when fully damaged the material can still carry compressive loads (crumbles are being compressed together), but can no longer carry any tensile or shear loads. To include this, the 4$^{\text{th}}$ order resin stiffness matrix is written as

$$
{}^4\mathbf{C}_r = \begin{cases} K\mathbf{I}\mathbf{I} + 2(1-D_r)G\left({}^4\mathbf{I} - \frac{1}{3}\mathbf{I}\mathbf{I}\right) & \text{for} \quad \varepsilon_{r,vol} \le 0 \\ (1-D_r)K\mathbf{I}\mathbf{I} + 2(1-D_r)G\left({}^4\mathbf{I} - \frac{1}{3}\mathbf{I}\mathbf{I}\right) & \text{for} \quad \varepsilon_{r,vol} > 0 \end{cases}, \text{ Equation 6}
$$

where **I** and ${}^4\mathbf{I}$ are the second and fourth-order unit tensors, respectively, K and G are the bulk and shear modulus, respectively, and D_r is the resin damage parameter.

2.1.5 Nonlocal damage theory

When a material gets damaged, part of the material can no longer carry any loads. Due to this the effective stiffness of the material decreases. Analyses with such softening behavior are normally very sensitive to mesh-dependency. To elevate this in Abaqus the characteristic length methods is available which for most cases can (partly) alleviate the mesh-dependency. A more general, but computationally less efficient, method for alleviating mesh-dependency is a nonlocal damage theory (e.g. Pijaudier-Cabot and Bazant, 1987; Bazant and Pijaudier-Cobot, 1988; Comi, 2001). In the non-local damage theory the local strain ε that determines the damage initiation is replaced by a nonlocal strain $\bar{\varepsilon}$. This nonlocal strain is taken as a weighted average of the strain within a volume *V*.

$$
\bar{\varepsilon}(\vec{x}) = \frac{1}{V}\int_V g(\vec{\xi})\varepsilon(\vec{x}+\vec{\xi})dV = \frac{\int_{i=1}^{n} V(\vec{\xi}_i)\exp\left(-\frac{\vec{\xi}_i^2}{2l^2}\right)\varepsilon_{,i}(\vec{\xi}_i)}{\int_{i=1}^{n} V(\vec{\xi}_i)\exp\left(-\frac{\vec{\xi}_i^2}{2l^2}\right)}, \text{ Equation 7}
$$

where l is the length scale of the material, V is the volume of punt i with a distance $\vec{\xi}_i$ from the current location $\vec{x}$.

For failure in composites, next to alleviating mesh-dependency there is another reason to use a non-local method. As mentioned in the previous paragraph compressive fiber failure is generally assumed to occur via micro buckling of the fibers. For micro buckling to occur, high strains or stresses should be present over certain length of the fiber. Hence, very local stress or strain peaks will probably not lead to micro buckling. As the nonlocal method uses an average strain over a certain area, it automatically filters out these very local strain peaks.

2.1.6 Implementation in Abaqus

The material model as discussed in the previous section (including the nonlocal damage theory) has been implemented in Abaqus/Standard using the user-subroutines UMAT and USDFLD. This implementation is schematically depicted in Figure 5. In increment 0 for all integration points all neighboring integration points within the influence volume (*V* in Equation 7) are determined. In increment 1 the local fiber and resin strains are determined in the subroutine UMAT. In the next increment these local strains are used to determine the nonlocal strain in the subroutine USDFLD using Equation 7. These nonlocal strains are then normalized by the local strains (Note that these are the normalized nonlocal strains from the previous increment). These normalized strains are transferred to the subroutine UMAT, where they are multiplied with the current local strains. The resulting nonlocal strain is used for the damage laws. This is repeated for all other increments. Hence, for determining the amount of damage the strain distributions from the previous increments are used, but the magnitudes are based on the current strains. Due to this a semi-implicit scheme is obtained, which is believed to be more accurate than a purely explicit scheme.

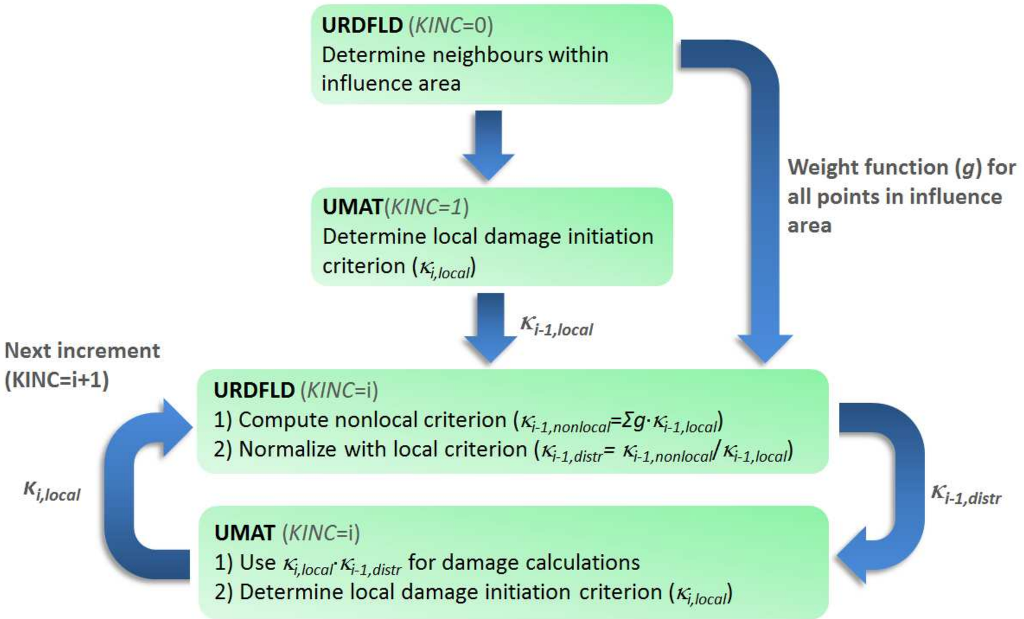

Figure 5. Schematic of the implementation of the non-local theory in Abaqus/Standard.

2.2 Delaminations

The initiation and growth of delaminations in composites is mainly governed by the transverse shear stresses (τ_{13}, τ_{23}). Apart from these transverse shear stresses the out-of-plane stresses play an important role. Compressive out-of-plane stresses are known to inhibit the initiation and growth of delaminations while tensile out-of-plane stresses are known to promote the initiation and growth of delaminations (Lecuyer and Engrand, 1992). A law for damage initiation based on the above assumptions is given by

$$\frac{\max(\tau_{1,3},\tau_{2,3})}{F_{tvsh}}+\beta\sigma_{33}\geq 1, \text{ Equation 8}$$

where F_{tvsh} is the transverse shear strength and β a positive constant. To implement this damage law in Abaqus/Standard the maximum stress criterion is used.

$$\left|\frac{\tau_{13}}{F_{13}}\right|,\left|\frac{\tau_{23}}{F_{23}}\right|,\left|\frac{\sigma_{33}}{F_{33}}\right| \geq 1, \text{ Equation 9}$$

To implement Equation 8 into Equation 9 G_{33} has to be set to an infinite value, and F_{13} and F_{23} have to be made dependent on the out-of-plane stress (σ_{33}). To make F_{13} and F_{23} dependent on the out-of-plane stress (σ_{33}) first Equation 8 has to be rewritten to

$$\frac{\max(\tau_{13},\tau_{23})}{\bar{F}_{tvsh}(\sigma_{33})} = \frac{\max(\tau_{13},\tau_{23})}{F_{tvsh} - \beta\,\sigma_{33}} \geq 1, \text{ Equation 10}$$

By setting the first field variable equal to σ_{33}, the effective transverse shear strength $\bar{F}_{tvsh}$ can be made dependent on σ_{33}. To set the first field variable equal to σ_{33}, σ_{33} first has to be written to the .FIL-file using the keyword

```
*EL FILE, elset=name, position=averaged at nodes
S
```

Using the subroutine URDFIL the values σ_{33} (obtained from the .FIL file) can be stored in a common block. In the subroutine UFIELD these the values σ_{33} are then retrieved from the common block and the first field variable is set equal to σ_{33}. In Abaqus/CAE maximum stress damage initiation criteria is then made dependent of this first field variable as shown in Figure 6.

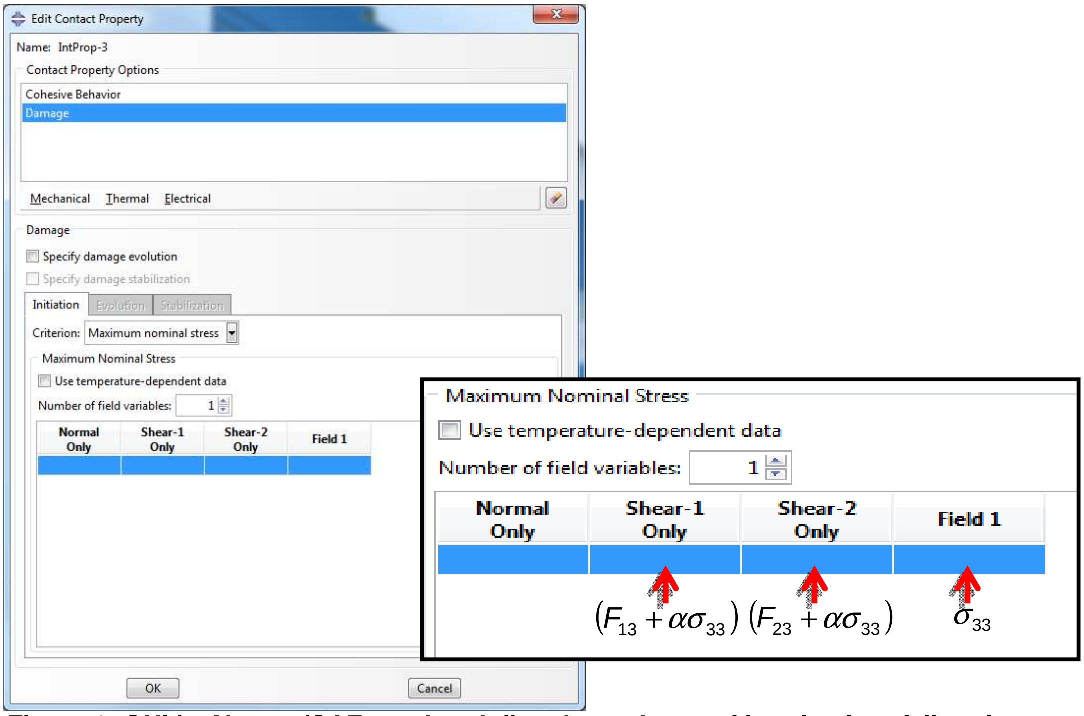

Figure 6. GUI in Abaqus/CAE used to define dependency of interlaminar failure law on σ_{33}.

2.3 Tested examples

2.3.1 In-plane shear

The in-plane shear tests were performed according to ASTM D3518 (see Figure 7). The tested specimens had dimensions of 270×25×3.87 mm and a layup of $[45°,-45°]_6$. The FEA model to mimic this test consisted of 6480 C3D8R elements with enhanced hourglass control. Due to symmetry only half of the sample was modeled. Each ply was modeled as a separate element layer. Boundary conditions were chosen such that the mimic they test conditions most accurately.

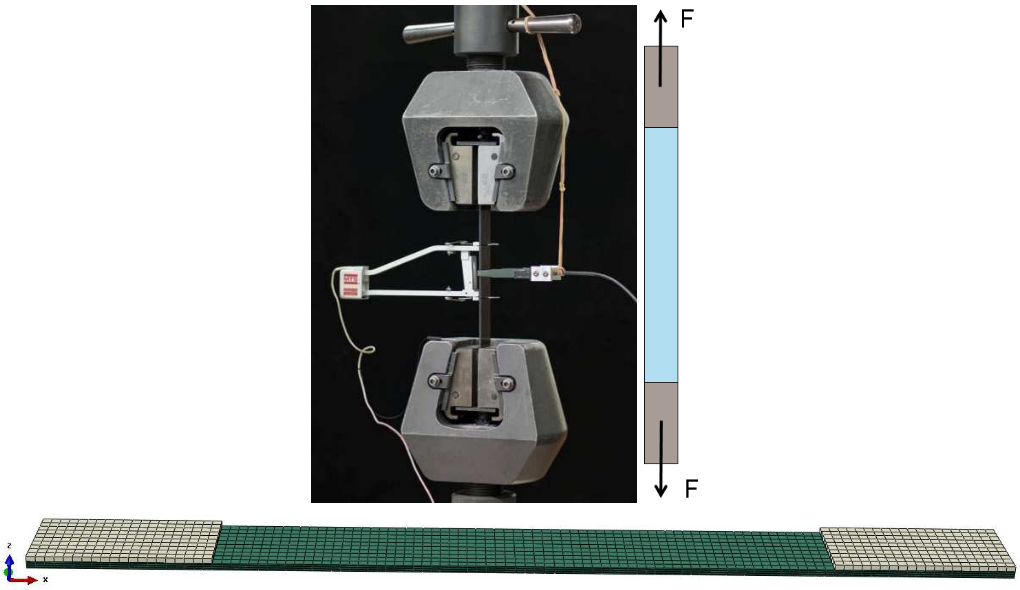

Figure 7. Top-Left) Photograph of in-plane shear test setup; Top-Right) Schematic of open hole in-plane shear test; Bottom) FEA mesh.

2.3.2 Inter-laminar shear

The inter-laminar shear tests were performed according to ASTM D2344 (see Figure 8). Two different configurations were tested: 1) tested specimens had dimensions of 27×15.6×1.89 mm and a layup of $[0°]_6$; 2) tested specimens had dimensions of 27×15×3.87 mm and a layup of $[0°, 90°]_6$. The FEA models consisted of 1512 and 3360 C3D8R elements with enhanced hourglass control, respectively. Due to symmetry, in the FEA models only a quarter of the total sample was modeled. Each ply was modeled as a separate element layer. The layers were tied together using cohesive surfaces. Damage initiation and growth behavior was including in the material description of the cohesive surfaces to model possible delaminations (see paragraph 2.2). For the contact between the support/loading rollers and the composite part surface-to-surface finite-sliding contact was used. For the cohesive surfaces between the plies surface-to-surface small-sliding contact was used. Boundary conditions were chosen such that they mimic the test conditions most accurately.

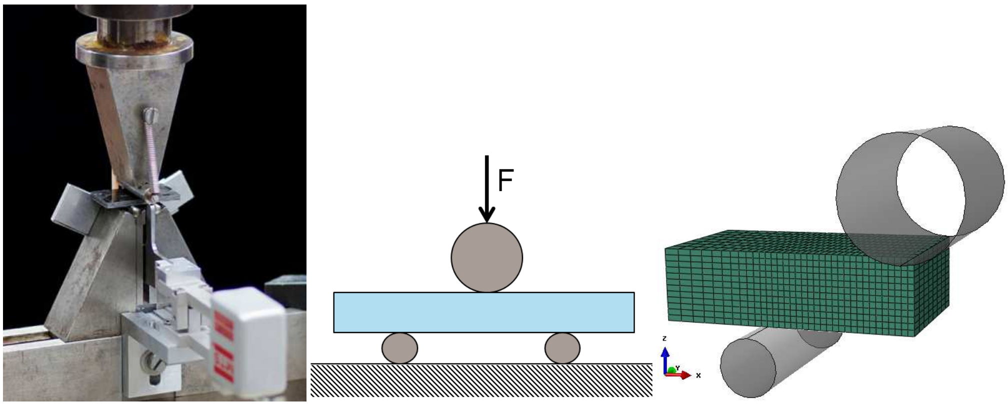

Figure 8. Left) Photograph of interlaminar shear test setup; Middle) Schematic of open hole interlaminar shear test; Bottom) FEA mesh.

2.3.3 Open hole compression

The open hole compression tests were performed according to ASTM D6484-9 (see Figure 10). The tested specimens had dimensions of 60×45×3.87 mm and a layup of $[45^\circ/-45^\circ/90^\circ/45^\circ/-45^\circ/0^\circ]_s$. The open hole had a diameter of 12.7 mm. The FEA model consisted of 4786 C3D8R elements with enhanced hourglass control. Due to symmetry, in the FEA models only half of the total sample was modeled. Each ply was modeled as a separate element layer. The layers were tied together using cohesive surfaces. Damage initiation and growth behavior was including in the material description of the cohesive surfaces to model possible delaminations (see paragraph 2.2). Surface-to-surface small-sliding contact was used for the cohesive surfaces. For the cohesive surfaces between the plies surface-to-surface small-sliding contact was used. Boundary conditions were chosen such that they mimic the test conditions most accurately.

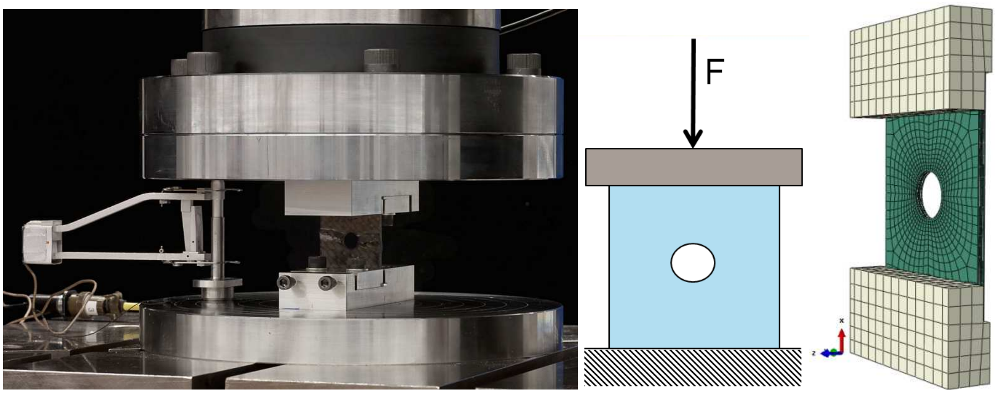

Figure 9. Left) Photograph of open hole compression test setup; Middle) Schematic of open hole compression test; Right) FEA mesh.

2.3.4 Bearing

The bearing tests were performed according to ASTM D5961-09 (see Figure 9). The tested specimens had dimensions of 60×45×3.87 mm and a layup of $[45°/-45°/0_2°/90°/0°]_s$. The loading pin had a diameter of 12.7 mm. The FEA model consisted of 5466 C3D8R elements with enhanced hourglass control (composite plate), and 4946 C3D10M elements (pin). Due to symmetry, in the FEA models only half of the total sample was modeled. Each ply was modeled as a separate element layer. The layers were tied together using cohesive surfaces. Damage initiation and growth behavior was including in the material description of the cohesive surfaces to model possible delaminations (see paragraph 2.2). For the contact between the loading pin and the composite part surface-to-surface finite-sliding contact was used. For the cohesive surfaces between the plies surface-to-surface small-sliding contact was used. Boundary conditions were chosen such that they mimic the test conditions most accurately.

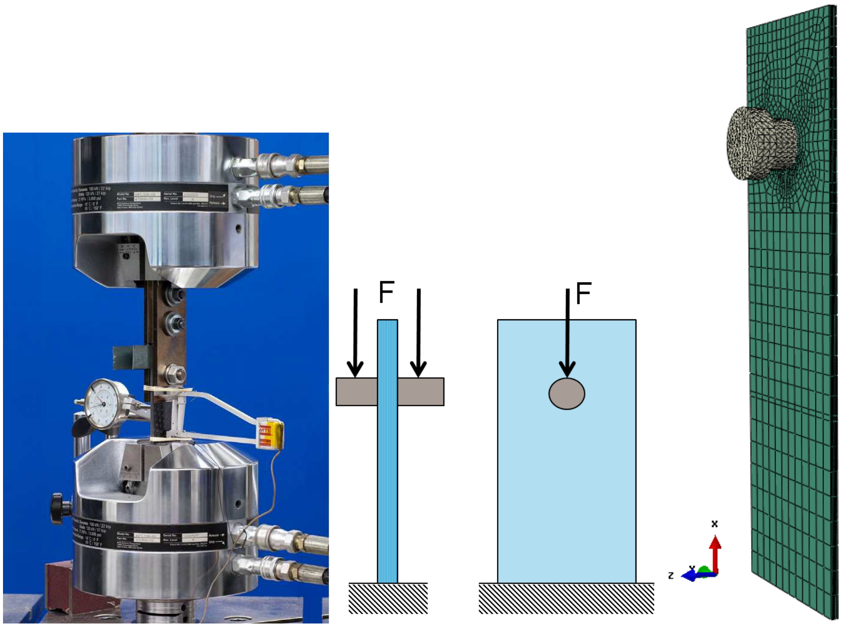

Figure 10. Left) Photograph of bearing test setup; Middle) Schematic of bearing test; Right) FEA mesh.

3. Results

3.1 In-plane shear

3.1.1 Traditional method

A typical stress strain curve of an in-plane shear test is given in Figure 11. As traditional models are linear elastic they cannot predict the nonlinear stress-strain behavior of the test. Traditionally the stiffness for composite models is based on the initial linear part of the stress-strain curve (see Figure 11). When using this stiffness the material stiffness for most strains is overestimated. This error increases with increasing strain. In traditional models the in-plane shear strength is used for most failure criteria. As can be seen in Figure 11, the failure strain is then greatly underestimated.

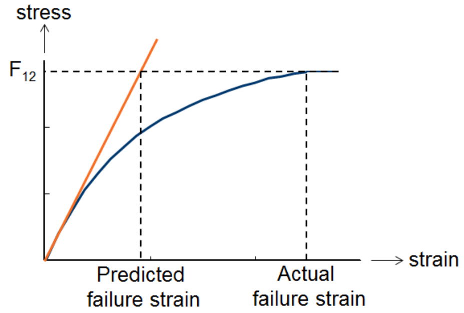

Figure 11. stress-strain curve of in-plane shear test (blue) along with stress-strain curve of traditional composite models (orange).

3.1.2 Current method

As can be seen in Figure 12 the force-strain response is captured very by the FEA model. Also the failure location is captured very well (Figure 13)

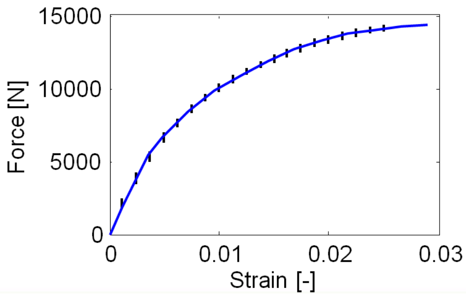

Figure 12. Left) force-strain curve of in-plane shear test. Vertical lines are the mean test values ± 1 standard deviation, the blue solid line is the FEA response.

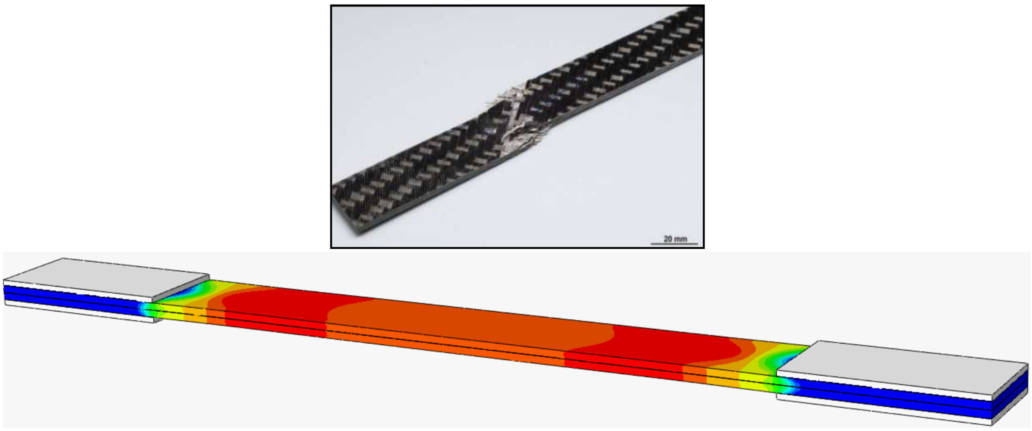

Figure 13. Top) failed in-plane shear coupon; Bottom) Predicted resin damage distribution at moment of failure (red=D=1; blue=D=0).

3.2 Inter-laminar shear

3.2.1 Traditional method

The test results showed a different behavior for the two tested configurations (Figure 14). The 0°/90°-samples showed a more brittle fracture compared to the 0°-samples. Moreover the interlaminar strength of the 0°/90°-samples was approximately 29% lower. For traditional methods a single value for the interlaminar shear strength is normally used. Based on the current results it is questionable what strength should be used for this, and how well it can be used to predict failure for other configurations.

3.2.2 Current method

In Figure 14 the response of the FEA model with the new material model is given. Although the material parameters have only been manually optimized it can already be seen that the model predicts a more brittle fracture for the 0°/90°-samples compared to the 0°-samples, as was seen in the test. For both configurations also the failure load was predicted relatively well.

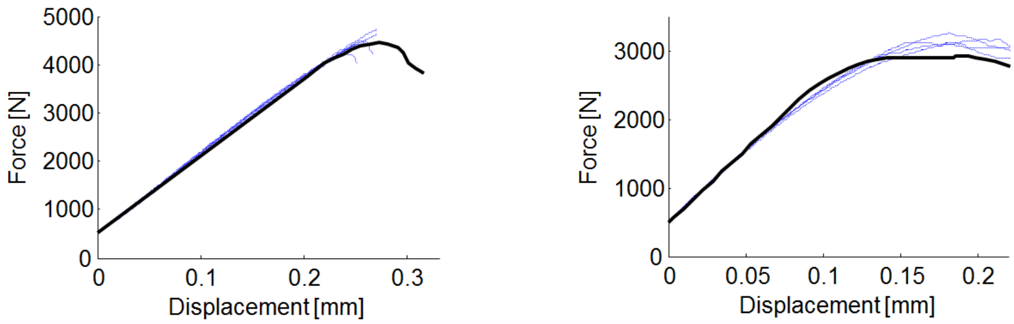

Figure 14. Force-displacement curves of interlaminar shear tests. Left) 0-90 layup;)Right) 0 layup. (blue lines = test data; black line = FEA results).

In Figure 15 the predicted delaminations at the failure load are given.

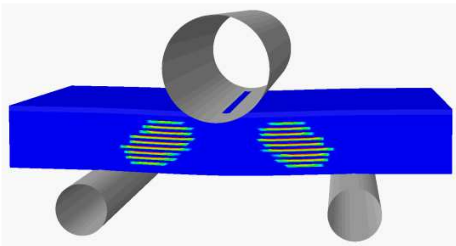

Figure 15. Predicted delaminations at maximum load (red=D=1; blue=D=0).

3.3 Open hole compression

3.3.1 Traditional method

In the traditional analyses methods failure of a composite is predicted by failure criteria like "maximum stress", "Hashin", "Tsai-Hill" or "Puck". When the values of these criteria have exceeded a value of 1, the composite is assumed to have failed. In Figure 17 the values of the maximum stress criterion are given for an FEA simulation in which the experimentally measured failure load is applied. As can be seen in Figure 16, the maximum value of the maximum stress criterion is approximately 2. This means that the FEA prediction under predicts the failure load of this test by a factor 2.

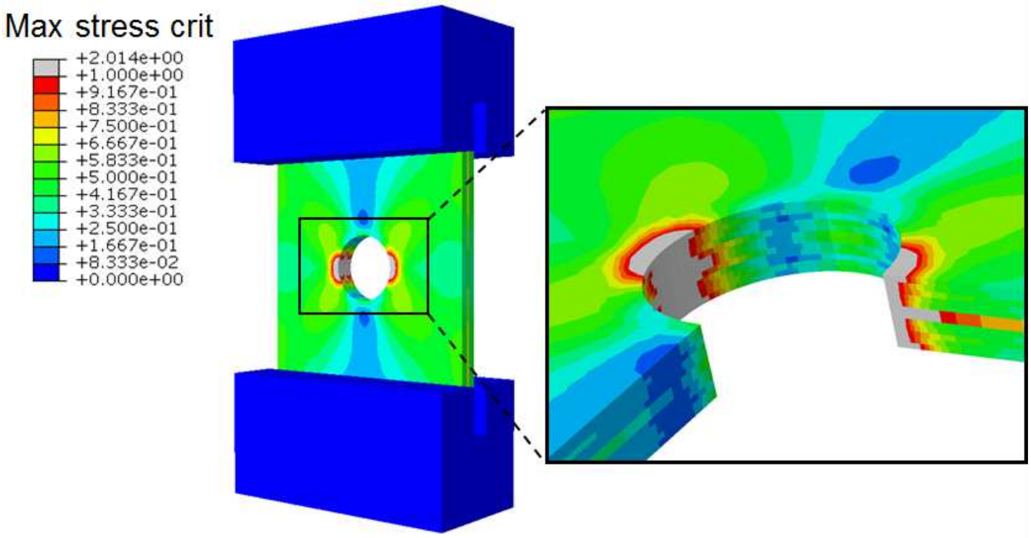

Figure 16. Maximimum stress values at the open hole compression failure load.

3.3.2 Current method

In the model presented in section 2 the damage initiation and progression of both the resin and the fibers is included. The failure load predicted with this model was 3.8% lower than the experimentally measured failure load, and falls nicely in within the ± 1 standard deviation range. In Figure 17 the predicted fiber and resin damage is given at the failure load. This corresponds very well with the failure mode seen in the tested specimens.

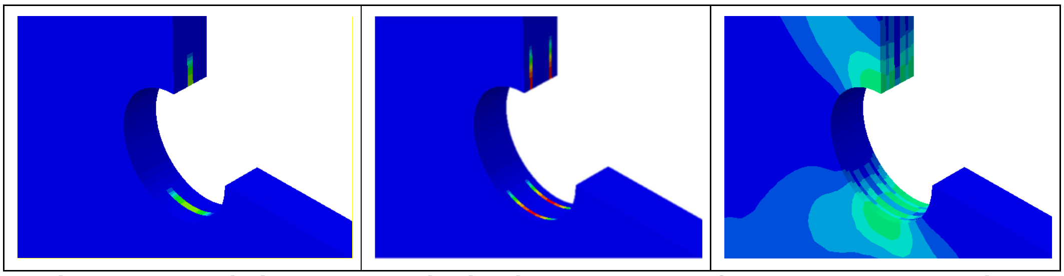

Figure 17. Prediction damage distribution at moment of open hole compression failure. Left) Warp fiber damage; Middle) Weft fiber damage; Right) Resin damage (red:D=1; blue:D=0).

3.4 Bearing

3.4.1 Traditional method

In Figure 18 the values of the maximum stress criterion are given for an FEA simulation in which the experimentally measured failure load is applied. As can be seen in Figure 17, the maximum value of the maximum stress criterion is approximately 2. This means that also for this test the traditional FEA prediction under predicts the failure load of this test by a factor 2.

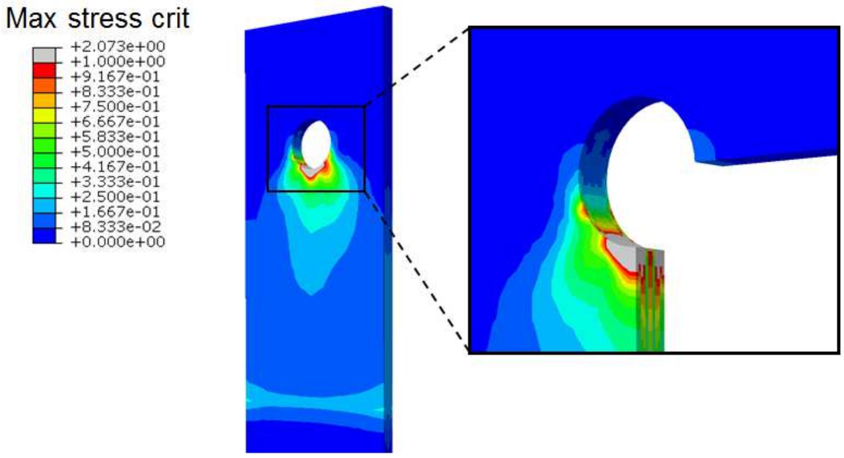

Figure 18. Maximimum stress values at the bearing failure load.

3.4.2 Current method

In the model presented in section 2 the damage initiation and progression of both the resin and the fibers is included. The failure load predicted with this model was 1.8% lower than the experimentally measured failure load, and falls nicely in within the ± 1 standard deviation range.

In Figure 19 the prediction fiber and resin damage is given at the failure load. This corresponds very well with the failure mode seen in the tested specimens. In Figure 20 the predicted deformation around the hole is given at the failure load. Clear delaminations can be seen between the outer plies. These delaminations can also be seen in the tested specimens.

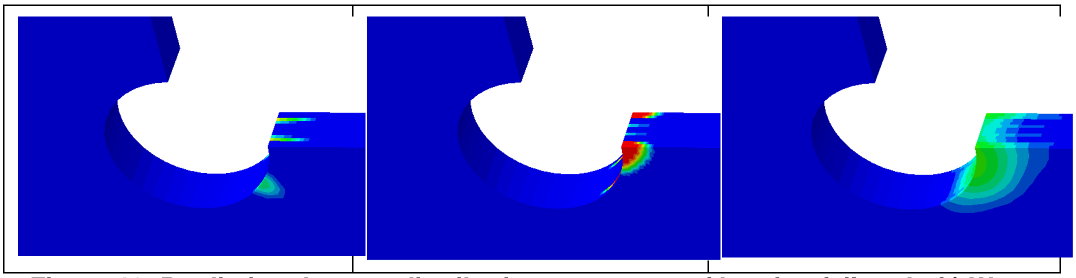

Figure 19. Prediction damage distribution at moment of bearing failure Left) Warp fiber damage; Middle) Weft fiber damage; Right) Resin damage (red:D=1; blue:D=0).

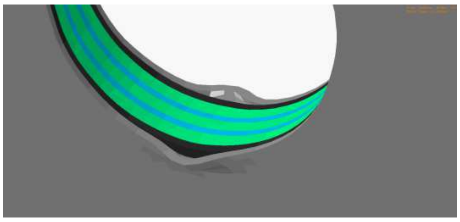

Figure 20. Delaminations after a bearing failure (scale factor of 10))

4. Discussion

The goal of the current study was to extend our previously developed fiber-reinforced composite model (Wilson, 2011) such that is can also accurately predict the failure of composites around stress concentrations. Therefore in the current study we have extended our material model to include non-local damage mechanics (including damage evolution), and more realistic (physics based) damage laws for (compressive) fiber damage. We have also added damage initiation criterion for the onset of damage in cohesive surfaces (delaminations) based on both transverse shear stresses and out-of-plane stresses.

As shown traditional methods for modeling composites do not include the nonlinear stress-strain behavior of the resin. Due to this the stiffness at higher strains is over predicted, and the failure strain is under predicted. With the material model presented in this article both the mechanical and failure behavior in in-plane and interlaminar shear tests can be predicted very well.

The presented interlaminar shear test data showed that specimens with a different layup (and thickness) gave different interlaminar shear strengths. This shows that a strength measured with a specific layup and thickness, is probably not representative for composite parts or sections with a different layup or thickness. The model presented in this paper could predict the behavior of both configurations with the same set of material parameters, and is therefore suitable for predicting the behavior other composites with a different layup or thickness as well.

One of the main limitations of the traditional analyses methods is that they cannot predict failure of composites around stress concentrations. As shown is this article the predicted failure strain can be underestimated by a factor of 2. The extension to our material model presented in this article now enables us to also accurately predict the moment of failure and failure mode (initiation and growth of fiber damage, resin damage and delaminations) around stress concentrations (open hole compression and bearing element tests). This makes it suitable for the accurate predictions of failure in any complex shaped composite part.

Currently this model has only been compared coupon and element test data. Although this was very successful, validation on (sub-)component level is needed to fully validate this approach.

5. References

1. Wilson.,W., Virtual testing of composites using Abaqus., 2011 SIMULIA Customer Conference, Conference Proceedings, May 17-19, 2011 [1]
2. Chang, F. et al., Failure of Composite Laminates Containing Pin Loaded Holes, Journal of Composite Materials. vol. 18, 255-278, 1984
3. Whitworth, H. A., et al., Failure analysis of composite pin loaded joints., Composite Structures, vol. 59, 261–266, 2003
4. Lecuyer, F., Engrand, D., A methodology for the identification of a criterion for delamination initiation, JNC8:751-762, 1992
5. Pijaudier-Cabot, T.G.P., Bazant, Z.P. Nonlocal damage theory, J. Engng. Mech. (ASCE), Vol. 113, pp.1512–1533, 1987
6. Bazant, Z.P., Pijaudier-Cobot, T.G.P., Nonlocal continuum damage, localization instability and convergence, J. Appl. Mech., Vol. 55, pp.287–293, 1988
7. Comi, C., A non-local model with tension and compression damage mechanisms, Eur. J. Mech. A/Solids, Vol. 20, pp.1–22. 2001